IEICE TRANS. COMMUN., VOL.E91–B, NO.9 SEPTEMBER 2008

PAPER

Sampling Rate Selection for Fractional Sampling in OFDM

Haruki NISHIMURA[†a)], **Mamiko INAMORI**[†b)], *Student Members*, *and* **Yukitoshi SANADA**[†c)], *Member*

SUMMARY Through fractional sampling, it is possible to separate multipath components and achieve diversity gain. However, power consumption grows as the sampling rate increases. This paper proposes a novel scheme for OFDM systems that selects the sampling rate according to the channel's frequency response. Numerical results through computer simulation show that the proposed sampling rate selection scheme reduces power consumption by reducing oversampling ratio when delay spread is small.

key words: *software defined radio, cognitive radio, fractional sampling, IEEE802.11a/g, OFDM, multipath diversity*

1. Introduction

Nowadays, various wireless communication systems, including cellular systems, WLAN systems, etc., are widely employed. A multiband/multimode terminal is desirable in order to enable anywhere anytime connectivity [1]. However, since the receivers utilize different frequency bands and modulation schemes, different hardwares are necessary to implement them. Because of the various standards in different generations and regions, it is impossible to support all of those standards with one terminal. Therefore, to solve this problem, Software-Defined Radio (SDR) techniques have been investigated. In the ideal SDR, the most of receiving process is carried out in reconfigurable devices such as digital signal processors (DSPs) or field programmable gate arrays (FPGAs). This will make it possible to use one terminal to support any modulation schemes, generations, and regions [2].

The key components of the SDR techniques are the devices from the RF front-end to the analogue-to-digital converter (ADC). A variety of architectures has been proposed to realize the SDR. For example, an RF sampling reception scheme has also been proposed recently [3], [4]. In the RF sampling receiver architecture, the received signal is sampled at the radio frequency (RF). Those samples are input to the averaging filter for decimation. Therefore, by selecting the decimation factor, it is possible to choose the oversampling ratio of the baseband signal.

On the other hand, a fractional sampling (FS) technique in OFDM has been proposed [5]. Through FS, the received baseband signal is sampled with the rate higher than the Nyquist rate in order to achieve diversity gain. However, as the sampling rate increases, the power consumption grows due to the use of multiple demodulators.

In this paper, a sampling rate selection scheme according to frequency response of the channel is proposed. The proposed scheme reduces power consumption by decreasing the sampling rate when the delay spread is small.

This paper is organized as follows. Section 2 describes the system model. Section 3 shows the numerical results through computer simulation. Section 4 gives our conclusions.

2. System Model

2.1 Fractional Sampling

A block diagram of an OFDM system with FS is shown in Fig. 1. Suppose the information symbol on the kth subcarrier is $s[k](k = 0, \ldots, N-1)$, the OFDM symbol is then given as

$$u[n] = \frac{1}{\sqrt{N}} \sum_{k=0}^{N-1} s[k] e^{j\frac{2\pi nk}{N}} \tag{1}$$

where $n(n = 0, 1, \ldots, N-1)$ is the time index. A cyclic prefix is appended before transmission as shown in Fig. 2. N_{GI} is the number of the sample points per guard interval.

The baseband signal at the output of the filter is given by $x(t) = \sum_{n=0}^{N+N_{\mathrm{GI}}-1} u[n]p(t - nT_s)$ where $p(t)$ is the impulse response of the baseband filter and T_s is the symbol duration. This signal is upconverted and transmitted through a

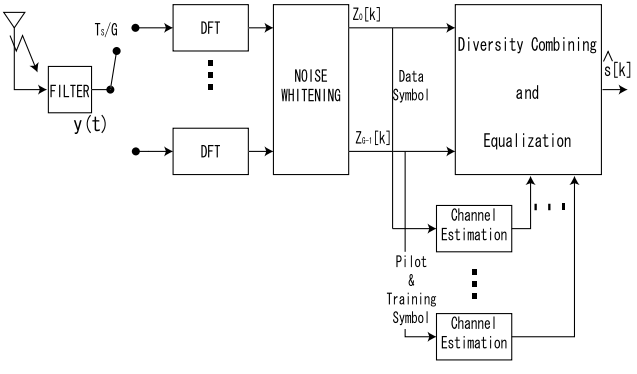

Fig. 1 OFDM receiver using FS.

Manuscript received October 10, 2007.
Manuscript revised April 26, 2008.

[†]The authors are with the Dept. of Electronics and Electrical Engineering, Keio University, Yokohama-shi, 223-8522 Japan.
a) E-mail: harunishimuraki@snd.elec.keio.ac.jp
b) E-mail: mamiko@snd.elec.keio.ac.jp
c) E-mail: sanada@elec.keio.ac.jp

DOI: 10.1093/ietcom/e91–b.9.2876

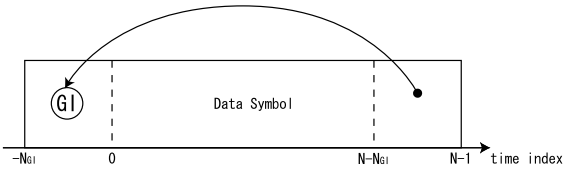

Fig. 2 OFDM symbol structure.

multipath channel with an impulse response $c(t)$. The received signal after the down conversion is given as

$$y(t) = \sum_{n=0}^{N+N_{\mathrm{GI}}-1} u[n]h(t - nT_s) + v(t) \tag{2}$$

where $h(t)$ is the impulse response of the composite channel and is given by $h(t) := p(t) \star c(t) \star p(-t)$ and $v(t)$ is the additive Gaussian noise filtered at the receiver. For the multipath channel, $h(t)$ can be expressed in a baseband form as

$$h(t) = \sum_{i=0}^{N_m-1} \alpha_i p_2(t - \tau_i) \tag{3}$$

where $p_2(t) := p(t) \star p(-t)$ is the deterministic correlation of $p(t)$ ($\star$ indicates convolution operator) and satisfies Nyquist's property. It is assumed that the channel in Eq. (3) has N_m path components, α_i is the amplitude that is time-invariant during one OFDM symbol (quasistatic channel model), and τ_i is the path delay. If $y(t)$ is sampled at the rate of T_s/G, where G is the oversampling ratio, its polyphase components can be expressed as

$$y_g[n] = \sum_{l=0}^{N+N_{\mathrm{GI}}-1} u[l]h_g[n - l] + v_g[n], g = 0, \ldots, G - 1 \tag{4}$$

where $y_g[n]$, $h_g[n]$, and $v_g[n]$ are polynomials of sampled $y(t)$, $h(t)$, and $v(t)$, respectively, and are expressed as

$$\begin{aligned} y_g[n] &:= y(nT_s + gT_s/G + \delta(G)), \\ h_g[n] &:= h(nT_s + gT_s/G + \delta(G)), \\ v_g[n] &:= v(nT_s + gT_s/G + \delta(G)) \end{aligned}$$

where $\delta(G)$ is the initial timing of the samples. Since $\delta(G) \geq 0$, n should start from -1 and the following condition is satisfied in order to avoid intersymbol interference.

$$nT_S + gT_S/G + \delta(G) \leq (N - 1)T_S. \tag{5}$$

After removing Guard Interval (GI) as shown in Fig. 3 and taking DFT at each subcarrier, the received symbol is given by

$$\mathbf{z}[k] = \mathbf{H}[k]s[k] + \mathbf{w}[k], \tag{6}$$

where $\mathbf{z}[k] = [z_0 \ldots z_{G-1}]^T, \mathbf{w}[k] = [w_0 \ldots w_{G-1}]^T$, and $\mathbf{H}[k] = [H_0 \ldots H_{G-1}]^T$ are $G \times 1$ column vectors, each gth component representing

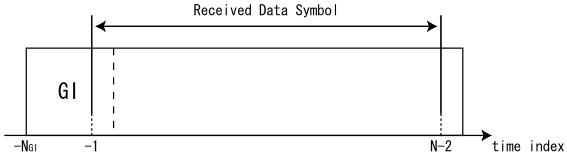

Fig. 3 Guard interval removal.

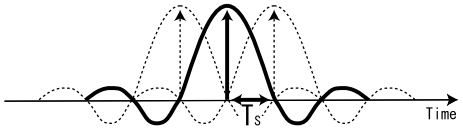

(a) Narrow band white noise($G = 1$)

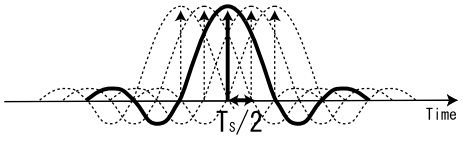

(b) Colored noise($G = 2$)

Fig. 4 Noise correlation through FS.

$$[\mathbf{z}[k]]_g := z_g[k] = \sum_{n=0}^{N-1} y_g[n]e^{-j\frac{2\pi kn}{N}}, \tag{7}$$

$$[\mathbf{w}[k]]_g := v_g[k] = \sum_{n=0}^{N-1} v_g[n]e^{-j\frac{2\pi kn}{N}}, \tag{8}$$

$$[\mathbf{H}[k]]_g := H_g[k] = \sum_{n=0}^{N-1} h_g[n]e^{-j\frac{2\pi kn}{N}}, \tag{9}$$

respectively.

As already stated, $v(t)$ in Eq. (2) is the filtered noise. It is well-known that when $v(t)$ is sampled at the baud rate of $1/T_s$, the samples of $v(t)$ are independent one another as shown in Fig. 4(a). However, when the sampling rate is multiple of the baud rate, the noise samples are colored. Therefore, it is necessary to whiten the colored noise samples as shown in Fig. 4(b).

In order to perform noise-whitening, it is necessary to calculate a $G \times G$ noise covariance matrix, $\mathbf{R}_w$, on each subcarrier. The (g_1, g_2)th element of the noise covariance matrix on the kth subcarrier is given as

$$\begin{aligned} &[\mathbf{R}_w[k]]_{g_1 g_2} \\ &\quad = E[w_{g1} w_{g2}^*] \\ &\quad = \sigma_v^2 \frac{1}{N} \sum_{n_1=0}^{N-1} \sum_{n_2=0}^{N-1} p_2((n_2 - n_1 + (g_2 - g_1)/G)T_s) \\ &\qquad\qquad \times e^{j\frac{2\pi k(n_2-n_1)}{N}} \end{aligned} \tag{10}$$

and multiplying both sides of Eq. (6) by $\mathbf{R}_w^{-\frac{1}{2}}[k]$ [5]

$$\mathbf{R}_w^{-\frac{1}{2}}[k]\mathbf{z}[k] = \mathbf{R}_w^{-\frac{1}{2}}[k](\mathbf{H}[k]s[k] + \mathbf{w}[k]), \quad (11)$$

$$\mathbf{z}'[k] = \mathbf{H}'[k]s[k] + \mathbf{w}'[k], \quad (12)$$

where $\mathbf{z}'[k] = \mathbf{R}_w^{-\frac{1}{2}}[k]\mathbf{z}[k]$, $\mathbf{H}'[k] = \mathbf{R}_w^{-\frac{1}{2}}[k]\mathbf{H}[k]$, and $\mathbf{w}'[k] = \mathbf{R}_w^{-\frac{1}{2}}[k]\mathbf{w}[k]$. With Eq. (11), noise-whitening can be achieved. Therefore, multiple outputs on each subcarrier are obtained through FS. Based on the channel response estimated by the preamble, those samples are combined to maximize the SNR expressed as the following equation [5],

$$\hat{s}[k] = \frac{\mathbf{H}'^H[k]\mathbf{z}'[k]}{\mathbf{H}'^H[k]\mathbf{H}'[k]} = \frac{(\mathbf{R}_w^{-\frac{1}{2}}[k]\mathbf{H}[k])^H(\mathbf{R}_w^{-\frac{1}{2}}[k]\mathbf{z}[k])}{(\mathbf{R}_w^{-\frac{1}{2}}[k]\mathbf{H}[k])^H(\mathbf{R}_w^{-\frac{1}{2}}[k]\mathbf{H}[k])}. \quad (13)$$

where $\{\cdot\}^H$ is the Hermitian operator.

2.2 Sampling Rate Selection

Though FS achieves diversity gain, it increases power consumption. In some channel conditions, the power of the received signal may be large enough to satisfy a required quality of the communication link without path diversity through FS. Therefore, in the proposed scheme, the sampling rate is selected in accordance with the frequency response of the channel. Also, the different sampling rate leads to the different response of the channel as indicated in Eq. (9). In the proposed scheme the sampling rate is selected as follows. Suppose the frequency response of the channel with the oversampling ratio of G at the kth subcarrier is expressed as follows.

$$P_G[k] = \mathbf{H}'^H[k]\mathbf{H}'[k]. \quad (14)$$

Figure 5 shows the frequency response of the channel interms of the subcarrier number. The most of the bit error occurs on the subcarrier with low frequency response. The large oversampling ratio of G boost the power of the channel response especially on the subcarriers which have low power frequency response in the case of small G. The oversampling ratio, G, is selected with the following criterion,

$$\max_G\{\min_k C_G P_G[k]\}, \quad (15)$$

where C_G is the coefficient for the oversampling ratio of G and

$$0 < C_G \leq 1.0.$$

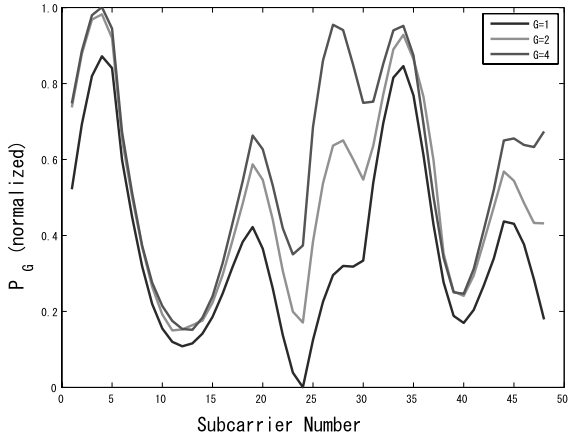

Fig. 5 Example of the frequency response of the channel.

3. Numerical Results

3.1 Simulation Conditions

Simulation conditions are presented in Table 1. In this simulation, the oversampling ratio G is selected among $\{1, 2, 4\}$.

The response of the channel is assumed to be constant during one OFDM packet. The structure of the OFDM packet for computer simulation is shown in Fig. 6.

Relevant to IEEE802.11a/g standard, the number of subcarriers, N, is 64 (48 subcarriers are for data symbols, 4 subcarriers are for pilot symbols, and the rests are null subcarriers) [6], [7]. For channel estimation, two symbols, T_1 and T_2 are used. The ideal channel estimation is assumed here. The oversampling ratio in the preamble period is fixed to $G = 4$. In the data period, the oversampling ratio is selected according to the criterion in Eq. (15). Reconfigurable ADCs are assumed [8]. This paper focuses on the average oversampling ratio in the data period as the length of the data

Table 1 Simulation conditions.

Modulation scheme	1st:QPSK, 16QAM, 64QAM 2nd:OFDM
FFT size	64
Number of subcarriers	64
Number of data subcarriers	48
Number of OFDM packets per trial	10000
Number of OFDM symbols per packet	100
Bandwidth of subcarriers	312.5 [kHz]
Preamble length (GI+Preamble)	1.6 + 6.4 [μs]
OFDM symbol length (GI+Data)	0.8 + 3.2 [μs]
Channel model	Rayleigh(16 path, equal gain), Indoor Residential A

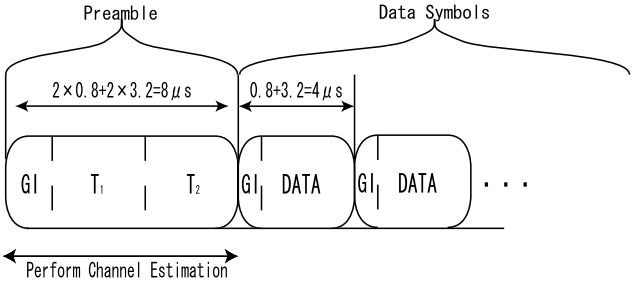

Fig. 6 OFDM packet structure for simulation.

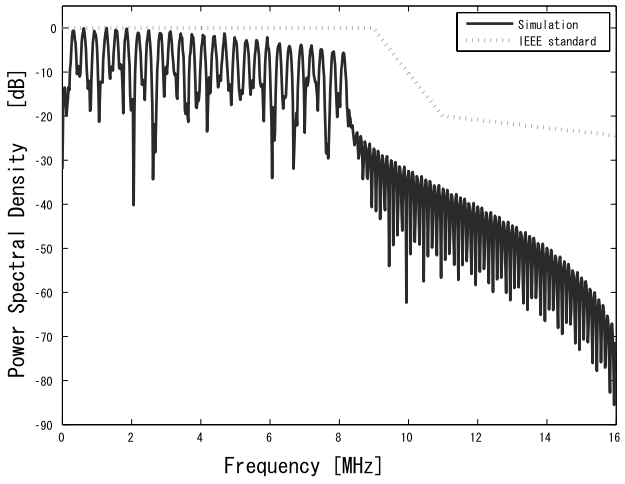

Fig. 7 Power spectrum density of the transmit signal.

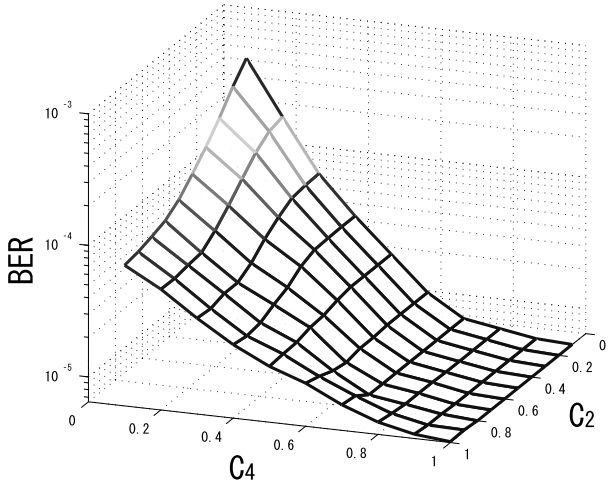

Fig. 8 16 path Rayleigh fading model (E_b/N_0 = 20 [dB]).

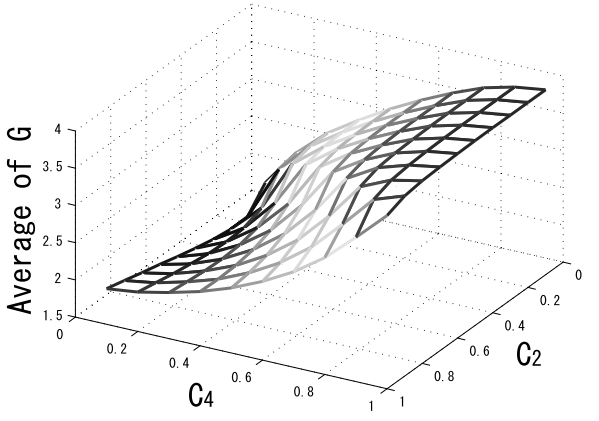

Fig. 9 16 path Rayleigh fading model (E_b/N_0 = 20 [dB]).

period is 100 OFDM symbols which is much larger than the preamble length. The total response of the transmitter and receiver filters are also assumed to be truncated sinc pulse with the duration of $2T_s$ [5]. As shown in Fig. 7, the spectrum of the transmitted signal filtered by the transmitter filter $p(t)$, satisfies the transmit spectrum mask defined in the IEEE802.11a standard [6].

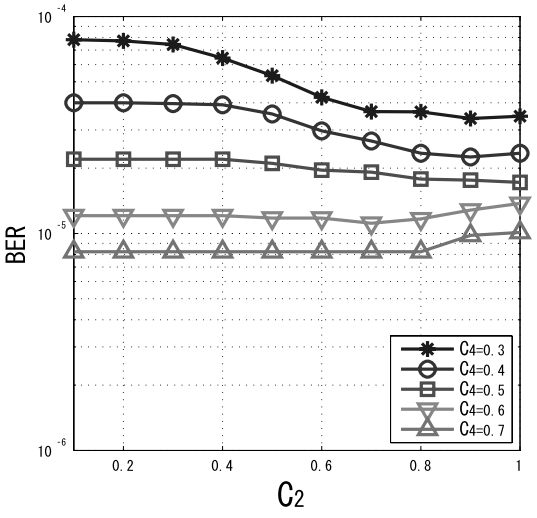

(a) BER

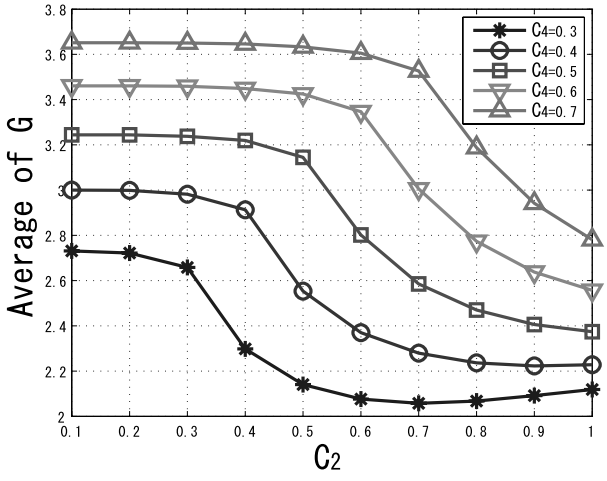

(b) Prob. of sampling rate selection

Fig. 10 16 path Rayleigh fading model (E_b/N_0 = 20 [dB]).

As the channel model, 16 path Rayleigh fading with uniform delay spread is assumed. Also, Indoor Residential A model in [9] is assumed, which has small delay spread.

3.2 16 path Rayleigh fading

Figure 8 shows the relationship between the BER and the coefficients, C_2 and C_4 (C_1 = 1.0). Figure 9 shows the average oversampling ratio versus the coefficients. As C_2 and C_4 increase, the BER reduces. However, as the BER performance improves, the average oversampling ratio, G, increases as shown in Fig. 9.

Figure 10(a) and (b) show the BER versus C_2 and the

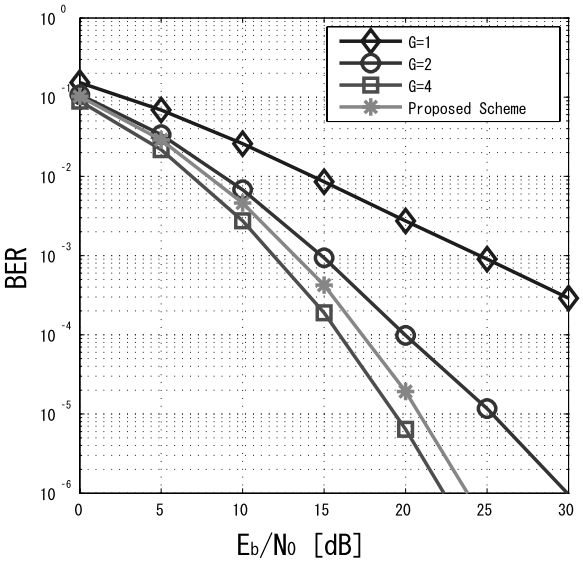

(a) BER

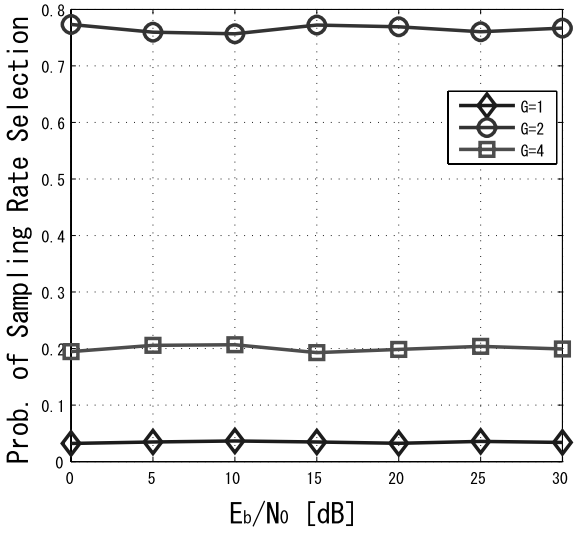

(b) Prob. of sampling rate selection

Fig. 11 16 path Rayleigh fading model ($C_2 = 1.0, C_4 = 0.5$).

Table 2 16 path Rayleigh fading model.

E_b/N_0 [dB]	Average of G
0	2.35
5	2.37
10	2.37
15	2.35
20	2.36
25	2.37
30	2.36

average of G versus C_2 when $0.3 \leq C_4 \leq 0.7$, respectively. It is clear that C_2 is relatively insensitive to the BER while it may reduce the average of G.

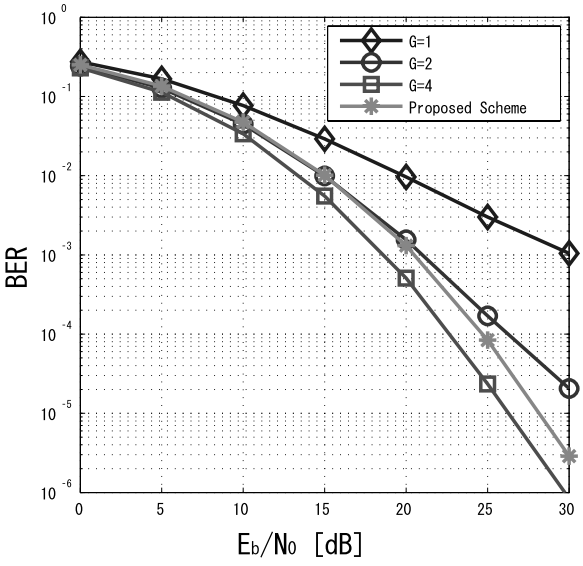

(a) BER

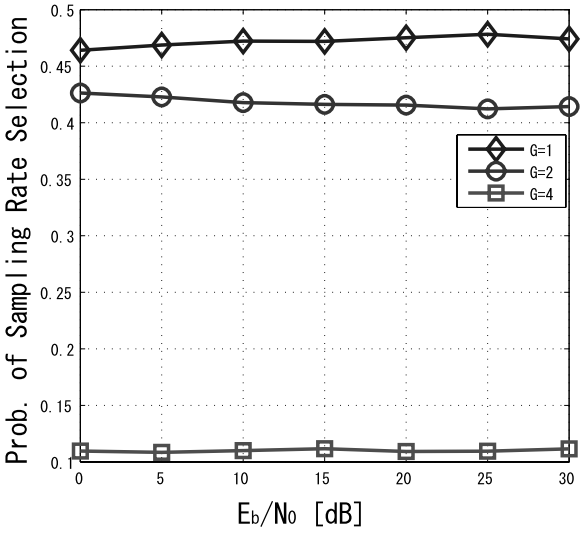

(b) Prob. of sampling rate selection

Fig. 12 Indoor Residential A ($C_2 = 0.7, C_4 = 0.5$).

Figures 11(a) and (b) show the BER curves obtained through FS and the probability of sampling rate selection, respectively. Here, C_2 and C_4 are set to 1.0 and 0.5. From Fig. 11(b), the probability of sampling rate selection is constant under different E_b/N_0 conditions. Table 2 shows the average oversampling ratio. From Fig. 11(a) and Table 2, while the proposed scheme reduces the average oversampling ratio by 40%, the BER curve is still close to that with $G = 4$.

3.3 Indoor Residential A

Indoor Residential A model has exponential delay profile

Table 3 Indoor Residential A.

E_b/N_0 [dB]	Average of G
0	1.75
5	1.74
10	1.74
15	1.75
20	1.74
25	1.74
30	1.74

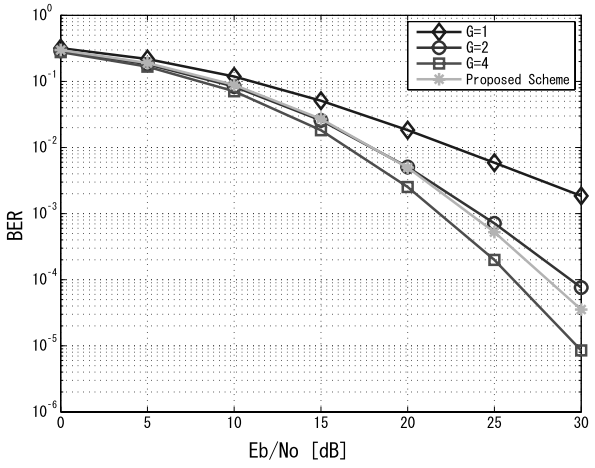

(a) 16QAM

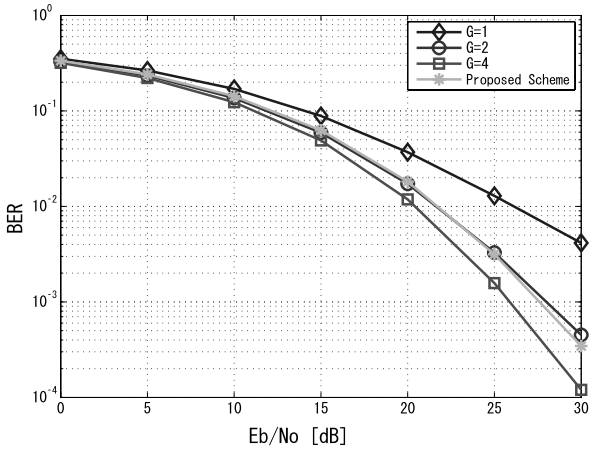

(b) 64QAM

Fig. 13 Indoor Residential A ($C_2 = 0.7, C_4 = 0.5$).

with the delay spread of 16 [ns]. Figures 12(a) and (b) show the BER versus E_b/N_0 and the probability of sampling rate versus E_b/N_0, respectively. Here, C_2 and C_4 are set to 0.7 and 0.5. Table 3 shows the average oversampling ratio. From Fig. 12(a), it is clear that the BER improvement with FS is less significant because of small delay spread. The oversampling ratio of 4 is hardly selected and the average oversampling ratio is less than 1.8. Thus, power consumption is significantly reduced when the delay spread is small. This because in Indoor Residential A model path diversity through FS is not effective since the power of the first arrival path is larger than the rest and the delay spread is small. On the same channel model, numerical results with higher modulation levels are shown in Figs. 13(a) and (b). In the both figures, the BER with the proposed scheme is better than that with $G = 2$. The average oversampling ratio is about 1.74 and is constant in terms of the different E_b/N_0.

4. Conclusions

In this paper, a sampling rate selection scheme for FS has been proposed for two typical channel models. The selection of the coefficient for each oversampling ratio depends on the channel models and required performance in terms of BER and power consumption. With the proposed scheme, the power consumption can be reduced significantly if the delay spread is small. When the delay spread is large, the BER performance can be improved while the power consumption is still saved with the proposed sampling rate selection scheme. For future work, the relationship between the coefficients for the oversampling rate and the other channel models will be clarified.

References

[1] R. Bagheri, A. Mirzaei, M.E. Heidari, S. Chehrazi, M. Lee, M. Mikhemar, W.K. Tang, and A.A. Abidi, "Software-defined radio receiver: Dream to reality," IEEE Commun. Mag. vol.44, no.8, pp.111–118, Aug. 2006.
[2] J. Mitola, "Technical challenges in the globalization of software radio," IEEE Commun. Mag., vol.37, no.2, pp.84–89, Feb. 1999.
[3] K. Muhammad, D. Leipold, B. Staszewski, Y.-C. Ho, C.M. Hung, K. Maggio, C. Fernando, T. Jung, J. Wallberg, J.-S. Koh, S. John, I. Deng, O. Moreira, R. Staszewski, R. Katz, and O. Friedman, "Discrete-time bluetooth receiver in a 0.13 μm digital CMOS process," ISSCC Dig. Tech. Papers, vol.1, pp.268–527, Feb. 2004.
[4] A. Matsuzawa, "Analog IC technologies for future wireless systems," IEICE Trans. Electron., vol.E89-C, no.4, pp.446–454, April 2006.
[5] C. Tepedelenlioĝlu and R. Challagulla, "Low-complexity multipath diversity through fractional sampling in OFDM," IEEE Trans. Signal Process., vol.52, no.11, pp.3104–3116, Nov. 2004.
[6] IEEE 802.11a-Part 11: Wireless LAN Medium Access Control (MAC) and Physical Layer (PHY) specifications; Highspeed Physical Layer in the 5GHz Band.
[7] IEEE 802.11g-Part 11: Wireless LAN Medium Access Control (MAC) and Physical Layer (PHY) specifications; Highspeed Physical Layer in the 2.4GHz Band.
[8] M. Anderson, K. Norling, A. Dreyfert, and J. Yuan, "A reconfigurable pipelined ADC in 0.18 μm CMOS," 2005 Symposium on VLSI Circuits Digest of Technical Papers.
[9] Joint Tecnical Committee of Committee T1 R1P1.4 and TIA TR46.3.3/TR45.4.4 on Wireless Access, "Draft final report on RF channel characterization," Paper no.JTC(AIR)/94.01.17-238R4, Jan. 1994.

Haruki Nishimura was born in Chiba, Japan in 1983. He received his B.E. degree in electronics engineering from Keio University, Japan in 2007. Since April 2007, he has been a graduate student in School of Integrated Design Engineering, Graduate School of Science and Technology, Keio University. His research interests are mainly concentrated on software defined radio.

Mamiko Inamori was born in Kagoshima, Japan in 1982. She received her B.E. and M.E. degrees in electronics engineering from Keio University, Japan in 2005 and 2007 respectively. Since April 2007, she has been a Ph.D. candidate in School of Integrated Design Engineering, Graduate School of Science and Technology, Keio University. Her research interests are mainly concentrated on software defined radio.

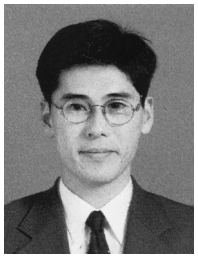

Yukitoshi Sanada was born in Tokyo in 1969. He received his B.E. degree in electrical engineering from Keio University, Yokohama Japan, his M.A.Sc. degree in electrical engineering from the University of Victoria, B.C., Canada, and his Ph.D. degree in electrical engineering from Keio University, Yokohama Japan, in 1992, 1995, and 1997, respectively. In 1997 he joined the Faculty of Engineering, Tokyo Institute of Technology as a Research Associate. In 2000 he jointed Advanced Telecommunication Laboratory, Sony Computer Science Laboratories, Inc, as an associate researcher. In 2001 he jointed Faculty of Science and Engineering, Keio University, where he is now an associate professor. He received the Young Engineer Award from IEICE Japan in 1997. His current research interest is in software defined radio and ultra wideband systems.